Unobtrusive Monitoring of Sensorimotor Performance in Ground-Based Functional Tasks

Hannah M. Weiss
KBR, Inc.
2101 E NASA Pkwy
Houston, TX 77058
Hannah.m.weiss@nasa.gov

Sarah C. Moudy
Aegis Aerospace, Inc.
2101 E NASA Pkwy
Houston, TX 77058
Sarah.c.moudy@nasa.gov

Scott J. Wood
National Aeronautics and Space Administration
2101 E NASA Pkwy
Houston, TX 77058
Scott.j.wood@nasa.gov

Abstract*— Astronauts returning from long-duration exposure to microgravity frequently exhibit alterations in sensorimotor function leading to postural imbalance, impaired locomotion, and operational challenges to manual control. Mission duration and individual responses often influence both the severity of performance decrements and the variability in adaptation timelines. Postflight disruptions during functional tasks are often detected through body-worn inertial measurement unit (IMU) devices. While IMU sensors are relatively compact, the long-term wear may lead to discomfort, displacement of the sensors on the body, and restrictions in movement or crew behavior. Although IMU data offers valuable insights from a research standpoint, interpreting changes in pre- and post-flight measures can be difficult for crew support personnel beyond the research domain, which can hinder the application to medical assessments and rehabilitation. Finally, the availability of inertial sensors in-flight is limited. There is a need for unobtrusive monitoring tools to improve our ability to monitor adaptation following gravitational transitions in various postflight evaluations and rehabilitation settings. Markerless motion capture is an evolving unobtrusive technology that builds upon decades of research with marker-based systems to provide 3D human pose estimation from multiple synchronized 2D camera views using deep learning algorithms. Markerless technology can revolutionize how data is captured pre- and post-flight and potentially in-flight during intravehicular activity by enabling pose estimation of multiple crew members from onboard camera hardware. The following paper presents an evaluation of a state-of-the-art commercial-off-the-shelf markerless motion capture system, Theia3D, compared to traditional IMU devices during various functional tasks and environmental conditions. Concurrent functional data are analyzed for nine participants of varying anthropometry. The analysis includes limited assessments of clothing, camera availability, and testing settings. The average RMSD was less than five degrees for all functional tasks evaluated in both a laboratory and field-testing location. The field-testing location, led to slightly higher deviations in head and trunk estimation. Functional tasks with more dynamic requirements resulted in larger deviations. The limited assessment of clothing indicates that the flight suit has minimal impact on the estimation accuracy of the head and torso. The development of visualization tools to enhance the application of the pose estimation output is also presented. These tools offer effective methods for anonymizing sensitive crew data, facilitating numerous applications across research, medical, and rehabilitation groups. The following work lays the foundation for future implementation leveraging markerless motion capture to assess the time course of recovery to baseline performance and provide insight for rehabilitation protocols to enhance crew readiness for the resumption of daily activities.

979-8-3503-5597-0/25/$31.00 ©2025 IEEE

Table of Contents

1. Introduction 1
2. Methods 2
3. Results 7
4. Discussion 9
5. Conclusion 11
Appendices 11
A. Tables 11
B. Figures 11
Acknowledgements 12
References 12
Biography 14

1. Introduction

Markerless motion capture (MMC) is an emerging technology that builds upon decades of research with marker-based motion capture systems [1], a process that requires notable setup time due to the need for manual marker placement on the human body to achieve accurate movement tracking. MMC systems, such as Theia3D (Theia Markerless Inc., Kingston, ON), provide three-dimensional human pose estimation from multiple synchronized two-dimensional camera views using deep learning neural network algorithms [2]. Following a calibration procedure, to determine the position and orientation of each camera, the deep learning algorithms are applied on a frame-by-frame basis to identify and track distinct anatomical landmarks on the human body. Markerless systems provide an unobtrusive and portable alternative to marker-based systems by eliminating the need for marker placement procedures and reducing hardware requirements to support data collection outside of laboratory settings.

For human spaceflight, MMC technology can revolutionize how data is captured during intravehicular activity by enabling unobtrusive monitoring capabilities and multi-subject tracking. MMC applied to in-cabin videos has the potential to support sensorimotor assessments, medical examinations, rehabilitation, training, behavior health, crew responses during Lunar ascent and descent, and inflight exercise evaluations. On the ground, the markerless technology can enable quicker and more unobtrusive assessments of crew members' sensorimotor performance before and after spaceflight, enhancing the capabilities of existing devices like inertial sensors during standardized sensorimotor tasks [3]. Adopting markerless technology could streamline sensorimotor evaluations and enhance crew support, however, further research is essential to understand the software's limitations and ensure the effective integration into crew assessments and rehabilitation strategies.

Previous spaceflight-related work includes the development of depth camera-based tools for resistive exercise during spaceflight [4], video-based ergonomic assessments for training in a microgravity analog environment [5], and a marker-based motion capture system for evaluating spacesuit performance underwater [6, 7]. More recently, Vu et al., [8] developed machine-learning solutions for automatic recognition of spacesuit motion from conventional video to enable quantification of suit kinematic patterns to optimize hardware and task designs. While the single-view camera approach offers approximate postural information adequate for certain scenarios, it is acknowledged that this method may face accuracy limitations due to camera distortion and the challenges of reconstructing 3D content from singular 2D views. In general, multi-view camera systems can substantially decrease occlusions and blur [9], enhancing the robustness of the algorithmic output and mitigating the limitations of single-view approaches. There are additional inherent challenges associated with ground-based and in-flight astronaut evaluations that may impact the tracking accuracy of MMC systems, including increased occlusions, smaller volumetric spaces, and restricted camera viewpoints. Further development and evaluation of multi-view MMC systems for spaceflight applications, including assessments of unsuited conditions, are essential to evaluate data quality and inform vehicle design and hardware for in-flight and ground integration.

Theia3D (Theia Markerless Inc., Kingston, ON) is a state-of-the-art MMC software that is continually assessed through an expanding array of research, including multiple comparison studies using marker-based motion capture across various functional tasks. Theia3D delivers notable accuracy in MMC full-body tracking while providing automated multi-subject capture from multiple synchronized camera views. Previous comparative analyses have demonstrated lower extremity kinematics and kinetic outcome measures of Theia3D matching closely with marker-based motion capture during functional activities of daily living and common exercises in sports and recreation. Estimation of ankle and knee joint angles have presented root mean square deviations (RMSD) of less than 5.9 degrees and joint centers locations within 2.5 cm for all joints except the hip (i.e., 3.6 cm) [10]. For upper extremity motions, Theia3D showed higher accuracy of 3D joint center position tracking of the shoulder and wrists (< 2.5 cm) than the elbow (> 3 cm) [11]. While the expanding body of research offers insights into the relative accuracy of Theia3D, most evaluations focus primarily on gait analysis. There is a need to assess the system on relevant spaceflight sensorimotor tasks and evaluate various body segments that are less explored in the literature, such as head-trunk coordination.

While marker-based systems are currently considered the gold-standard for validation and comparative analyses, both marker-based and markerless systems feature constraints and limitations to overall tracking quality. Comparing Theia3D to alternative motion tracking devices, such as inertial measurement units, could provide additional insight into the system's tracking accuracy. While IMUs also necessitate certain assumptions and exhibit their own tracking limitations, these devices could expand the literature focused on concurrent comparative analysis.

The quality and accuracy of MMC output data largely depend on the quality of the input data, which is influenced by hardware (e.g., number of cameras), environmental conditions (e.g., lighting, camera positions, occlusions), and the characteristics of the subjects (e.g., clothing) within the capture volume. Recent studies have assessed how clothing affects gait parameters, indicating that typical clothing styles have a minimal, potentially negligible impact on common gait metrics and the clinical interpretation for movement-related pathologies [12, 13]. More research is needed to investigate the effects of spaceflight-related clothing, such as flight suits during postflight evaluations, on the accuracy of motion tracking during sensorimotor assessments.

The current research performed evaluations of Theia3D in comparison to inertial sensors to assess the accuracy of head and trunk pose estimation during ground-based sensorimotor tasks relevant to spaceflight. The study also included a limited assessment of the influence of reduced camera availability, capture volume asymmetry, and loose clothing on tracking accuracy, simulating postflight testing environments where optimal conditions may not be met. A final objective of the study focused on creating visualization tools to enhance human pose estimation models for applications in astronaut rehabilitation and medical assessments.

2. METHODS

Participants

Nine healthy volunteers (mean ± SD [range]; height: 173.74 ± 9.13 cm, [154.94 - 187.96]) participated in this study across two distinct protocols. Participant selection involved two recruitment methods: three participants (one female, two male) performed tasks in the NASA Neuroscience Laboratory, while the remaining six participants (two female, four male) were recruited through the NASA Test Subject Screening Facility (TSSF) to participate in tasks related to a centrifuge study. Those recruited from the TSSF passed a Class III flight physical to enable eligibility for $+3G_x$ centrifuge exposure. The participants were informed of the procedures before participating. Those participating in the centrifuge study signed an informed consent approved by the NASA Johnson Space Center Institutional Review Board.

Participants reported no musculoskeletal or vestibular impairments at the time of testing.

Hardware and Software

The present evaluation study assessed the tracking capability of Theia3D (Theia Markerless Inc., Version 2023.1.0.3160p18) using the recommended Sony camera package. The camera package included eight Sony RX0 II cameras (Sony Group Corporation, Minato, Tokyo, Japan), eight compatible Sony wired control boxes, and a 10-port ethernet switch (Netgear, Inc., San Jose, CA). To ensure time synchronization, each camera was hard-wired via ethernet cable to the ethernet switch which was in turn connected to a computer for system initialization and data recording. Intrinsic lens calibrations were provided and used to correct for distortions and other visual artifacts of the cameras. Extrinsic calibrations were perform using a custom chessboard provided by the company to determine the position and orientation of each camera within the system relative to the global coordinate system.

The research operators followed the recommended procedures provided by the Theia Markerless support engineers for hardware setup and calibrations. Cameras were placed as close as possible to the capture volume, while ensuring the entire desired capture volume was visible from all camera views. Each camera was raised between 1.2 – 2.4 meters above the ground and unusual or partial subject views were avoided. Each capture volume aimed for a symmetrical camera array surrounding the entire space. The cameras were set to capture at 60 frames per second with a shutter speed of 1/500 to reduce motion blur.

Opal IMU devices (APDM Wearable Technologies, Inc.) were utilized for comparison to Theia3D. IMU sensors were worn on the head and the torso using adjustable fabric straps. The head IMU was place directly on the forehead with the screen facing outward. The torso IMU was placed at the level of the 10^{th} thoracic vertebrae on the back of the body for Protocol 1. During the Protocol 2 centrifuge study, the torso IMU was positioned on the front of the body for comfort due to extended time laying in a supine position at $+3G_x$.

Protocol 1: System Evaluation in a Laboratory Setting

The first protocol was designed to evaluate Theia3D in an optimal capture volume (Figure 1 top image) with three subjects of varying anthropometry (i.e., 165.10, 180.34, and 188.96 cm in height) while wearing normal clothing. The regular attire was not extremely loose nor tight to the body.[3]

The participants performed three functional tasks commonly implemented postflight for assessing astronaut's sensorimotor performance, known as the Sensorimotor Standard Measures. These tasks include a Sit-to-Stand task (S2S), a Cone Turn task (CT), and Tandem Walking task (TW) [3].

Figure 1. Markerless motion capture volumes. Top: Protocol 1 laboratory setting with eight cameras. Bottom: Protocol 2 field testing with six cameras at the Aerospace Environment Protections Laboratory (KBR, Inc., San Antonio, TX).

For the S2S task, the participants were instructed to sit upright in a chair facing forward with a neutral head position. When given a stand command by the operator, the participant would stand as quickly and safely as possible. This task was performed twice by the three participants, once with no restrictions and a second time with their head voluntarily locked to their torso during the motion (termed S2S fixed) (Figure 3). The second instance was performed to mimic observed postflight alterations in head-trunk coordination after long duration (> 6 months) missions to the International Space Station [14].

The CT task required the participants to walk straight towards and around a cone (5.08 cm high and 15.24 cm in diameter) placed on the floor while rotating in a counterclockwise motion, thereby performing a 180-degree turn towards one's left shoulder. Similar to the S2S task, the CT was performed under two distinct conditions. The first trial featured no functional restrictions. The second trial required the participants to voluntarily lock their head and torso once again (termed CT fixed), resulting in an en-bloc movement where the head and torso turned as a single unit around the cone (Figure 3). This turning strategy has been observed postflight by crew members experiencing sensorimotor disorientation and motion sickness symptoms.

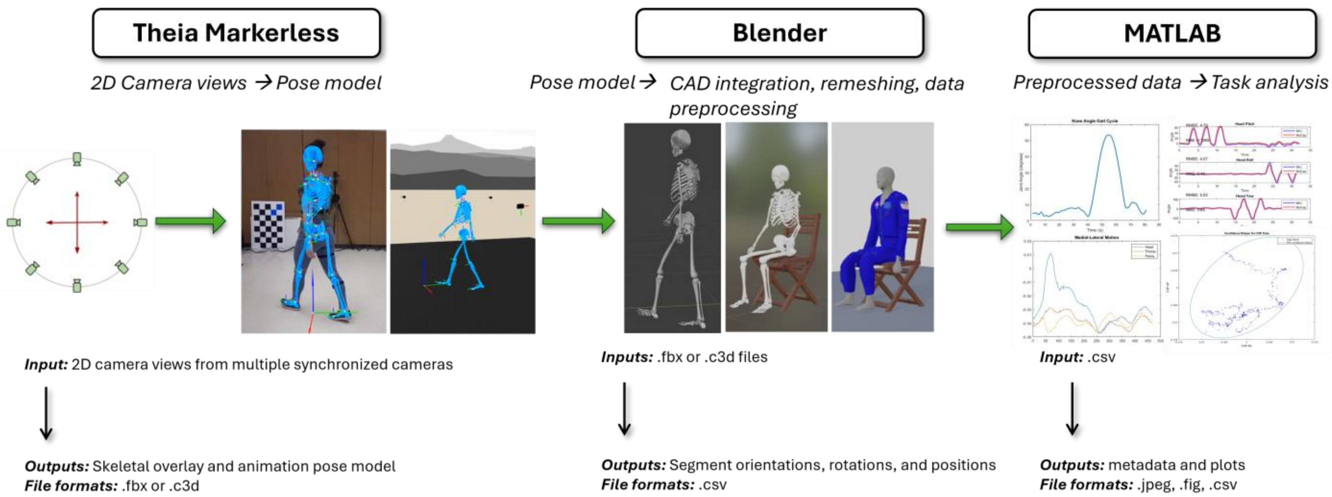

Figure 2. Analysis and visualization pipeline using Theia3D, Blender, and MATLAB. Raw 2D camera views, from multiple synchronized cameras, are processed for full-body 3D pose estimation to visualize and analyze human motion.

During the TW task, participants were instructed to walk heel-to-toe for 10 consecutive steps while maintaining their head in a neutral forward-facing posture. The task was performed with their eyes closed and arms crossed on their chest.

A secondary aim of the first protocol was to determine the impact of the participant's clothing, specifically a NASA flight suit, on the estimation accuracy of Theia3D. Two participants (180.34 and 187.96 cm in height) repeated three functional tasks (i.e., S2S, CT with head locked to torso, and TW eyes closed) while wearing a NASA flight suit, which are typically more loosely fit than streetwear and cover the entire arms, torso, and legs. Due to the limited sizes of flight suits available, one participant donned the flight suit to their hips and tied the arms of the suit around their waist at the belt level. The remaining participant wore the flight suit fully across the arms and legs. These suited trials were compared to the unsuited trials of the same functional tasks previously performed. For postflight testing, both flight suit configurations are commonly used and therefore were warranted within this limited evaluation.

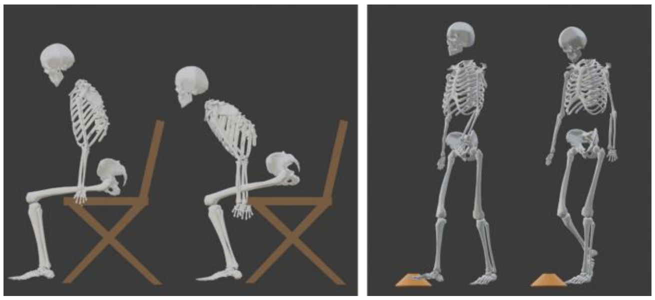

Figure 3. Unrestricted and restricted head-trunk locking variations of the functional tasks. Left: S2S. Right: CT.

Protocol 2: System Evaluation in a Field Test Setting

The second protocol was incorporated into a broader study design with alternative objectives relating to functional performance pre and post +3G_x centrifuge exposure, a validated spaceflight sensorimotor analog [15]. The present study utilized the testing protocol from the larger study to assess Theia3D in a less ideal but more realistic future testing environment, simulating postflight data collections with multiple subjects in the capture volume, fewer cameras, and an asymmetrical setup. The camera array featured six cameras rather than the eight utilized within the first protocol to determine the impact of a reduced camera set on the tracking accuracy of the system. The cameras were arranged in an oval configuration; however, some devices were positioned closer to the center of the region of interest than others and were partially obstructed by other hardware or room features (e.g., structural poles) (Figure 1 bottom image).

The participants performed nine assessment tasks, a novel centrifuge Susceptibility task, and two operationally relevant tasks that simulated extravehicular activity on the Lunar surface. The present analysis compares the accuracy of head and torso orientation across seven of the assessment tasks and the Susceptibility task prior to ingress into the centrifuge, i.e., prior to a sensorimotor disoriented state.

The assessment tasks included three postural balance tasks with three distinct foot stances (i.e., feet together, tandem stance, and single leg), variations of head movement (i.e., head rolling ear to shoulder or static) and differences in visual input (i.e., eyes open or closed). Each postural stance was held as long as possible up to 20 seconds while the participants arms were crossed over their chest. The tracking performance of Theia3D during feet adjacent and tandem stances with head rolling motion are presented as well was the single leg stance with eyes closed.

The Susceptibility task was designed to assess participant's susceptibility to sensorimotor disruption following sustained $+3G_x$ centrifuge exposure. During the Susceptibility task, participants stood in a tandem stance with arms crossed, head looking down at their feet, and eyes closed. Similar to the postural tasks, this stance was held for up to 20 seconds. The task would end if the participant fell out of the posture (e.g., arms uncrossed or feet no longer maintaining heel-to-toe contact) or the participant opened their eyes.

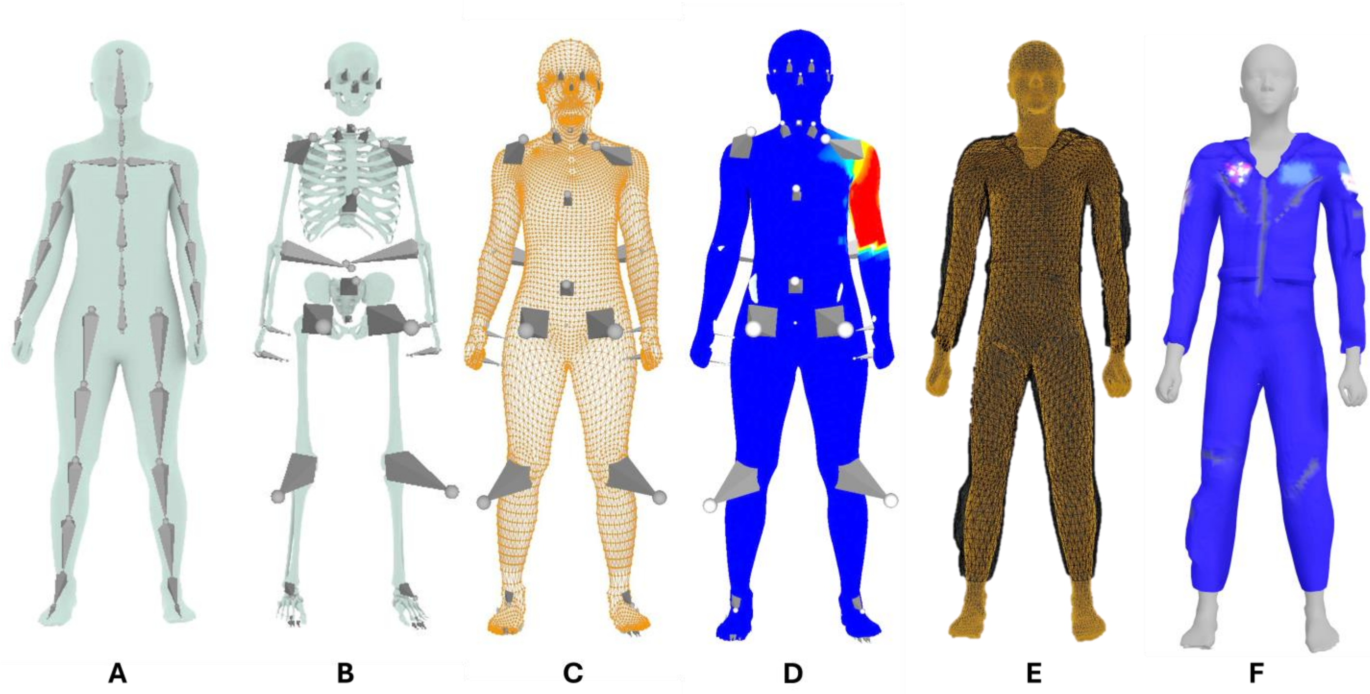

Figure 4. A) Human mesh and custom armature. B) Theia3D armature. C) Human mesh parented to the Theia3D armature. D) Updated weight paint for the left upper arm. E) Custom flight suit model parented to the Theia3D armature. F) Final human mesh and flight suit model paired to Theia3D armature with vertex painting.

The assessment tasks also featured clinical assessments such as the Four Square Step Test (FSST) [16] and the Step Test [17]. During the FSST participants quickly stepped both feet within four quadrants outlined by a cross object (2.54 cm high). Starting in the lower left quadrant, participants stepped in a clockwise followed by counterclockwise rotation. While performing the Step Test, participants tapped the ball of a single foot on the top of a block (7.5 cm high) and back to the floor at their starting position as many times as possible within fifteen seconds. The height of the step object was consistent with previous literature [17].

Two custom assessment tasks were also implemented and designed to challenge one's functional stability during leaning and turning motions and mimicked body mechanics that would be required during a Lunar surface extravehicular activity. The Obstacle Turn Task (OTT) required participants to step over a 30 cm foam obstacle, turn 180 degrees, step forward over the obstacle again followed by a 90-degree turn, and two side steps over the obstacle before returning to the original position. Both feet had to plant on either side of the obstacle after each turning motion was completed. The Kneel and Turn Task (KTT) required participants to step and then forward lunge with one knee on the ground. Upon kneeling, the participants were instructed to reach as far forward as possible and as far to the right and left as possible while holding a handheld flashlight tool before standing up. Participants were instructed to perform these two tasks as quickly as possible.

Comparative Analysis Methodology

Concurrent synchronous data was collected from the camera system and the IMU sensors for both protocols. Each dataset was processed to ensure consistent outputs, enabling a meaningful comparison. The full analysis procedure is outlined in Figure 2.

The raw two-dimensional camera views were extracted from each camera and organized in the appropriate structure to be used with the Theia3D software. Each calibration trial first was analyzed through Theia3D. The quality of each calibration trial was within the recommended limits for the diagonal and the angle root mean square error (RMSE). The error estimated for the length of the diagonals of the four outer corners of the chessboard relative to their known lengths was < 1mm (mean 0.84 mm) while error of the angle of the four outer corners of the chessboard relative to their known angle of 90 degrees was on average 0.13 mm.

To process each motion capture data trial, the respective calibration files were assigned to the appropriate dataset. The analysis procedure for each data trial within the Theia3D workspace included automatic 1) 2D tracking to detect people within each loaded video, 2) identification of individual people across the camera views and the assignment of a unique identifier, and 3) solving the 3D pose of each identified person. The third step scaled the embedded kinematic model and solved for the pose using inverse kinematics. The chosen Theia3D kinematic model consisted of a single full body kinematic chain comprised of the lower body, upper body, and the head. The full-body kinematic chain was selected instead of the default two-chain model (upper and lower body) to save the 3D poses in an FBX format, enabling further analysis and visualization.

The FBX files containing the 3D pose data and associated animations were imported into Blender, an open-source 3D computer graphics software tool. The Blender environment was utilized to create visualization tools described in the following section and to trim the data files and extract the orientation estimation of each body segment with respect to the global reference frame (i.e., north, west, up). Algorithms were created to save the raw quaternion data, the Euler representations, and the global positions for the center of mass of each skeletal segment in a CSV file for import into MATLAB (R2023a, The Mathworks, Inc., Natick, MA).

The inertial data was uploaded directly into MATLAB and processed through a custom-built function to transform the quaternion matrix (relative to a magnetic north, west, up reference frame) output from the ADPM software into Euler angles for comparison to the output from Theia3D.

Time synchronization of the motion capture and inertial sensor data was carried out algorithmically using known custom event marks capturing task start and end times from the IMU data and common signal characteristics (e.g., signal peaks). After temporal alignment of the signals, the RMSD and the magnitude-squared coherence (MSC) were evaluated separately for the head and torso orientation estimations. The RMSD is a measure of the average difference between the signal values across the entire time series offering an indication of their feature similarity. The MSC quantifies the strength of the linear relationship between two signals at different frequencies, representing how consistently the signal frequency components align. A smaller RMSD value exhibits greater similarity, indicating minimal deviations between the compared datasets, while a larger coherence suggests a stronger linear relationship between the signals at specific frequencies. Considering the small sample sizes within each protocol, statistical analyses was limited to descriptive statistics to characterize the differences.

Development of Visualization Tools

The present work also included the development of visualization tools to facilitate the comparison of crew performance before and after spaceflight, aiming to extend the technology beyond research to support crew rehabilitation efforts.

De-identification—Given the sensitivity of data related to astronauts, especially postflight in deconditioned states, a need for de-identification was recognized. Traditionally, video data is de-identified by blurring regions of the face. While this methodology is effective to some extent, it still leaves the possibility to identify the crew members based on other visible features. Markerless motion capture is well-suited for de-identification with skeletal pose models decoupled from the videos. However, when comparing pose models of multiple crew members simultaneously, it can be relatively easy to identify individuals based on their unique anthropometric features (e.g., stature).

A custom algorithm was developed to anthropometrically scale the 3D pose models to a common stature, such as 1.8 m (6 ft). The pose models are either scaled up or down to the common stature value. The desired common value can be modified as needed. This process is strictly implemented to support visual comparisons and de-identification and does not impact the quality of the data for research.

The FBX model exported from Theia3D, Figure 4B, features an armature, 3D meshes for each bone segment (e.g., rib cage, forearm, femur, etc.), and the animation data (e.g., quaternions of each body segment). The armature is a type of object used for rigging to control other objects similar to a marionette. The armature stores the rotations and positions for every frame of the data capture and applies the animation to the 3D skeletal meshes through a parent-child relationship in which movement, rotation, or scaling of the parent also influences the child objects. To scale the 3D pose model, visually represented by the skeletal bone meshes, the algorithm is applied to the armature thereby scaling the meshes as well.

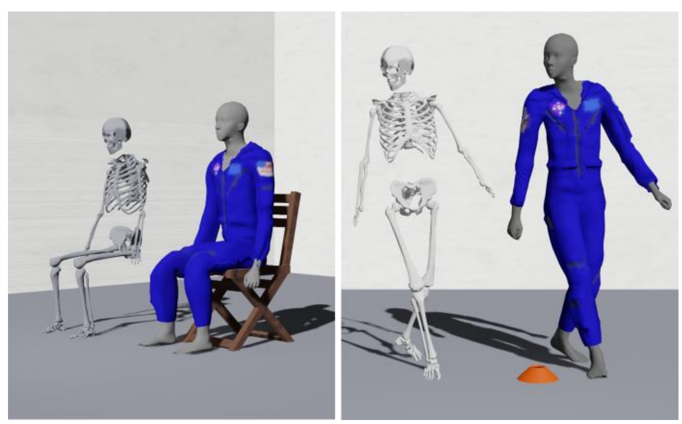

Figure 5. Visual reconstruction of task performance. Top: Sit-to-Stand task. Bottom: Cone Turn task.

Skeletal Meshing and Clothing Integration—While the skeletal 3D pose model accurately captures functional motion using rigid bone segments, a need for meshing the model with "skin" and a flight suit was recognized to enhance visualization. The skeletal pose model and the meshed model can be shown in parallel to provide a visual representation of both the rigid bone motion and a full reconstruction of the individual (Figure 5). Meshing skeletal armatures is often avoided due to the challenge of accurately representing real-life skin deformation, however tools and methods can be used to improve the visual deformation of a mesh.

Improving the relative influence of a bone segment on a mesh, termed vertex-weighting, can modify the associated impact of the bone's motion on the mesh. Weights are visualized on a 0 to 1 cold/hot color-coded scale, in which blue/cold represents closer to zero weighting and red/hot represents full weighting (Figure 4D). In vertex weighting, each vertex coordinate is influenced by a weighted combination of the linear transformations (or "linear blending") defined by the nearest bones in the armature [18]. Customizing the weights of the mesh to ensure there are no unreferenced vertices and adequate overlap of adjacent segments can support better visual animations of the mesh. Increasing the number of vertices (i.e., single 3D points) in the mesh (Figure 4C) and shading the object smooth rather than faceted can support a more skin-like appearance.

A generic human mesh, designed as a neutral representation without specific body type characteristics, was first re-meshed to increase the number of vertices from 10,000 to over 18,000. A custom armature was developed to repose the human mesh into a neutral anatomical position with the feet together and arms by the side to align with the neutral position of the Theia3D armature. The armature definition in Theia3D differs from the traditional armatures utilized in Blender requiring additional steps to apply the human mesh to the 3D pose model from Theia3D. Armatures are made of a collection of components, titled bones, containing three elements: the root, the body, and the tip. Traditionally the armature bones are linked root to tip like a real skeleton (Figure 4A). For example, the root of the forearm is linked to the tip of the upper arm to form the elbow joint. For Theia3D, the motion capture data appears to be entirely stored within root segment of the bone thereby defining a joint center and distal body segment by the root of a single bone (Figure 4B-D). Automatic weights, an option provided in Blender to speed up rigging using a common armature definition, was not applicable.

To apply the human mesh to the Theia3D model, the mesh was aligned to the joint centers of the armature and vertex re-weighting was applied to the vertices of the mesh. Each root of the Theia3D armature was manually associated with the appropriate body segment using weight paint to ensure the animated actions were properly applied to the mesh. For example, the left upper arm region of the human mesh was weighted to the left upper arm bone of the Theia3D armature (Figure 4D).

The flight suit mesh was parented and reweighted to the Theia3D armature following the same methodology. The flight suit was manually sculpted, textured, and vertex painted to replicate a NASA flight suit. To reduce the time required for rendering, the flight suit was created as a lower fidelity mesh. If higher fidelity is desired, the mesh can be re-meshed to increase the number of vertices.

CAD Integration—Custom computer-aided design (CAD) 3D models are introduced in the Blender environment to thoroughly recreate a visual representation of the task and the environmental conditions in which the tasks were performed. 3D models of the task objects, such as a chair for the S2S task or a cone for the CT task, can provide an improved visualization of subject motion relative to physical task objects (Figure 5).

3. RESULTS

Protocol 1: System Evaluation in a Laboratory Setting

When comparing Theia3D to the inertial sensors while wearing normal clothing, the mean RMSD of the head and torso were 2.32 ± 1.00 degrees (mean ± standard deviation) and 3.04 ± 0.41 degrees, respectively, averaged across all evaluated tasks and planes of motion (Appendix A Figure 13).

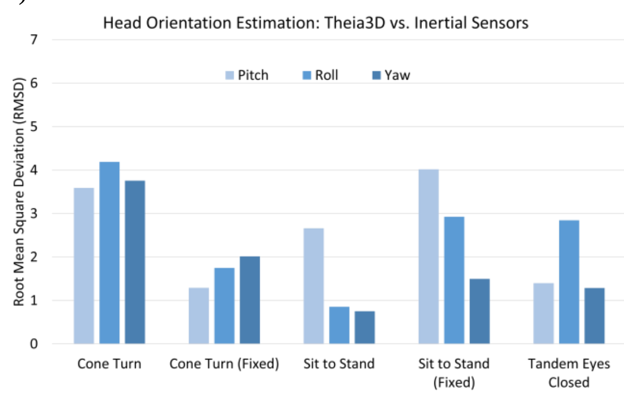

Figure 6. Protocol 1 (n = 3): Head orientation estimation comparison of Theia3D to inertial sensors.

Mean RMSD Euler Estimation—For both the head and torso, the estimation of pitch exhibited the largest RMSD when averaging across all tasks, 2.59 ± 1.24 degrees and 4.19 ± 1.31 degrees, respectively (Figure 13). The second largest RMSD for the head was in the roll plane of motion, 2.51 ± 1.27 degrees, followed by yaw, 1.86 ± 1.15 degrees. The second largest RMSD for the torso was in the yaw plane of motion, 3.39 ± 1.35 degrees, followed by roll, 1.53 ± 0.30 degrees.

Mean RMSD Within Task—For the head, the task that resulted in the highest RMSD between IMU and Theia3D, averaged across all three planes of motion (i.e., pitch, roll, and yaw), for the head was the unrestricted CT task in which the head and torso were permitted to move freely from each other, 3.85 ± 0.31 degrees (Figure 6). The variation of the CT task when the head and trunk were voluntarily locked together, resulted in the second lowest RMSD when considering the average across all three planes of motion, 1.69 ± 0.37 degrees. The S2S task, with unfixed head-trunk motion, yielded the lowest average deviation for the head when combining pitch, roll, and yaw deviations, 1.42 ± 1.07

degrees. For the torso, the S2S head locked to torso condition exhibited the largest average deviation across all three planes of motion, 3.56 ± 2.53 degrees (Figure 7). The unrestricted CT task presented the lowest average deviation in torso orientation estimation, 2.68 ± 1.34 degrees.

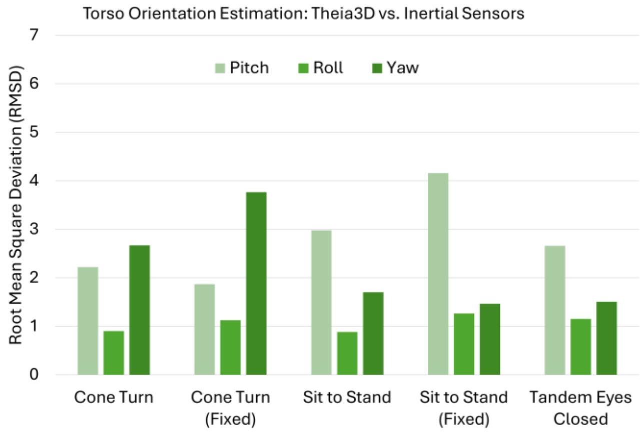

Figure 7. Protocol 1 (n = 3): Torso orientation estimation comparison of Theia3D to inertial sensors.

Mean Coherence—Considering the frequency domain, the head orientation exhibited the highest coherence between IMU and Theia3D in yaw, 0.66 ± 0.30, followed by pitch, 0.60 ± 0.20, and roll, 0.39 ± 0.09 across all the tasks evaluated. The unrestricted CT task showed the highest coherence of the head estimation, 0.75 ± 0.09, when considering all planes of motion and the TW eyes closed task resulted in the lowest coherence, 0.37 ± 0.04. The torso estimation yielded the highest coherence in pitch, 0.66 ± 0.29, followed by yaw, 0.55 ± 0.37, and then roll, 0.43 ± 0.12, across all tasks. When considering within task and across all planes of motion, the unrestricted CT task resulted in the highest coherence, 0.66 ± 0.26, and the TW eyes closed exhibited the lowest coherence, 0.40 ± 0.06. Appendix A provides a comprehensive overview of the coherence results for all the tasks evaluated.

Influence of Flight suit on Tracking Capability—The mean RMSD Euler estimation, averaged across tasks and planes of motion, for the head was 2.25 ± 0.33 degrees unsuited and 3.00 ± 0.47 degrees suited. The mean RSMD for the torso was 2.76 ± 1.35 degrees unsuited and 3.79 ± 2.76 degrees suited. The largest increase in the mean RMSD for the head estimation was observed in the yaw plane of motion (2.01 ± 0.33 degrees unsuited and 3.55 ± 3.41 degrees suited) (Figure 8). Similar results were identified for the torso, with an RMSD value of 2.83 ± 1.20 degrees unsuited and 4.60 ± 1.18 degrees suited along yaw motion. The CT task resulted in the largest change in RMSD (Appendix A Figure 11) suited for both the head (3.25 ± 1.88 degrees unsuited; 4.56 ± 2.81 degrees suited) and torso (2.95 ± 1.57 degrees unsuited; 4.29 ± 3.10 degrees suited) estimations when considering the mean deviation across all planes of motion (Appendix A Figure 12).

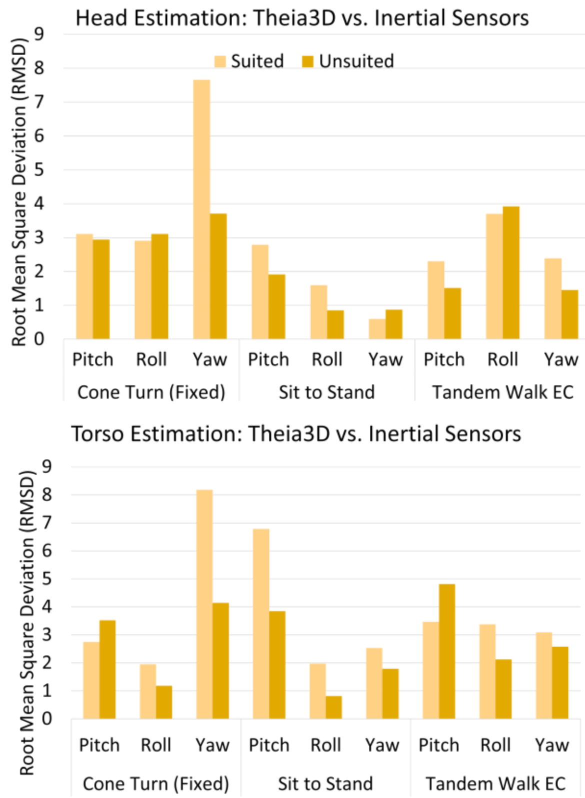

Figure 8. Unsuited vs. Suited RMSD comparisons for head and trunk orientation estimation with concurrent motion capture and inertial sensor data (n =2).

Protocol 2: System Evaluation in a Field Test Setting

Comparing the markerless motion capture to the inertial sensors, the mean RMSD of the head and torso were 4.89 ± 1.96 degrees and 4.33 ± 2.65 degrees, respectively, averaged across all evaluated tasks and planes of motion (Appendix A Figure 14).

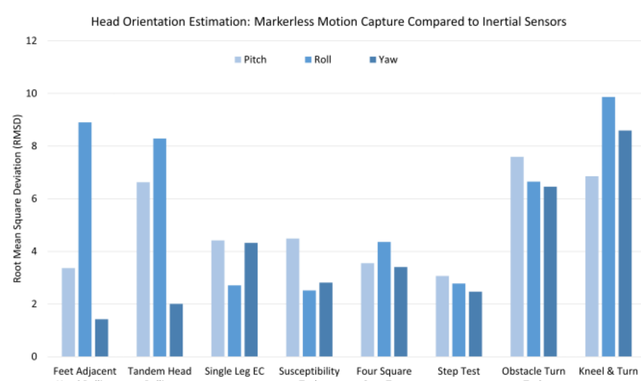

Figure 9. Protocol 2 (n = 6): Head orientation estimation comparison of Theia3D to inertial sensors.

Mean RMSD Euler Estimation—The average estimation across all tasks of head roll yielded the largest RMSD, 5.76 ± 3.04 degrees, followed by pitch, 4.99 ± 1.77 degrees, and yaw, 3.93 ± 2.45 degrees (Figure 9). Averaged across all tasks, the torso estimation exhibited the largest RMSD in yaw, 4.91 ± 3.36 degrees, followed by pitch, 4.42 ± 2.46 degrees and finally roll, 3.66 ± 2.39 degrees.

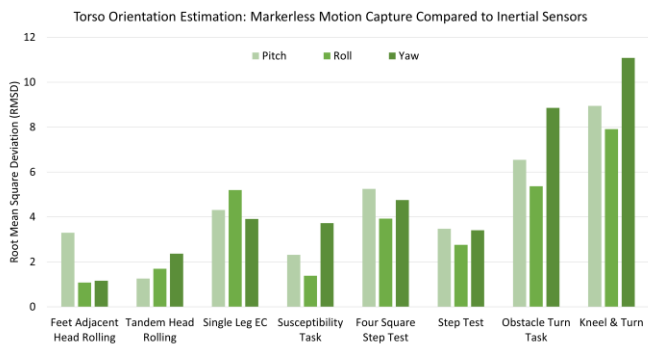

Figure 10. Protocol 2 (n = 6): Torso orientation estimation comparison of Theia3D to inertial sensors.

Mean RMSD Within Task—The more dynamic tasks, such as the OTT and the KTT, resulted in the largest RMSD values for the head estimation when considering the average deviation across all three planes of motion, 6.90 ± 0.61 degrees and 11.23 ± 3.24 degrees, respectively (Figure 9). In contrast, the Step Test and Susceptibility tasks, showed the lowest head RMSD considering all three planes of motion, 2.77 ± 0.30 degrees and 3.27 ± 1.06 degrees, respectively. For the torso, the OTT and KTT also exhibited the highest deviations of 6.92 ± 1.78 degrees and 9.31 ± 1.62 degrees, respectively. The tandem stance head rolling and feet adjacent head rolling tasks presented the lowest torso deviations of 1.77 ± 0.56 degrees and 1.85 ± 1.26 degrees, respectively (Figure 10).

Mean Coherence—In the frequency domain, the largest coherence value, averaged across tasks, was found in the estimations of head pitch, 0.40 ± 0.10, followed by yaw, 0.37 ± 0.20, and roll, 0.33 ± 0.10. For the torso, the yaw estimations yielded the highest coherence values, 0.42 ± 0.18, followed by pitch, 0.42 ± 0.20, and roll, 0.33 ± 0.16. Appendix A provides a comprehensive overview of the coherence results for all the tasks evaluated.

4. DISCUSSION

The results indicate the mean deviation between Theia3D and inertial sensors for the head and torso pose estimation, across all tasks performed and planes of motions, were less than five degrees for both testing protocols. The data also suggests the functional demands of a particular task influences the estimation accuracy of Theia3D where more dynamic motion may introduce less tracking accuracy. Tasks in which the head and torso was relatively stationary in global space, e.g., postural tasks, such as Step Test or the Susceptibility task, showed lower deviations values. In contrast, tasks that featured more motion and ambulation, such as the CT or KTT, exhibited higher deviation values. MMC algorithms are often known to struggle when tracking rotating, contorted, or non-upright individuals compared to normal upright motions such as walking. The difficulty can be attributed to most of the training datasets used within the algorithm comprising upright standing data and the inherent difficulties identifying human motion when body segments are occluding each other. Theia3D currently provides a functionality to run an alternative algorithm optimized to track inverted individuals, for example while performing a handstand. The tracking ability of these systems are expected to improve as the technology begins to mature and additional training datasets, including non-upright motions, are provided.

Although the two protocols assessed different assessment tasks, the functional characteristics regarding postural control during static and dynamic activities were similar. The results show that reducing the number of cameras from eight to six, combined with a non-symmetrical capture volume and the presence of more individuals and occlusions, led to slightly greater average deviations of head and trunk angle estimations between Theia3D and inertial sensors. The results suggest that the data accuracy in suboptimal environments remains within an acceptable margin of deviation compared to nominal conditions, indicating potential for future field applications.

Additional research is needed to establish the acceptable level of measurement variation, considering the intended data application. As a reference, RMSD values exceeding five degrees are typically viewed as clinically significant and could potentially distort clinical interpretations [19, 20]. Although a five-degree clinical threshold is commonly used for lower-limb evaluations across various systems, patient populations, or repeated intrasubject testing, the threshold may not be appropriate for head and trunk estimations. From a sensorimotor spaceflight perspective, the motion and orientation of a crew member's head can offer valuable insights into postflight recovery after vestibular readaptation to a gravitational environment. Immediately postflight, the positioning of the head relative to the torso and global space has been observed to exhibit noticeable changes and diverse coordination strategies [14, 21, 22]. In this context, a tracking error greater than five degrees could affect the interpretation of astronaut recovery and potentially misguide recommendations for operational readiness or rehabilitation. Alternative composite measures assessing the spatial coordination of the head and trunk may be less impacted if the tracking error is consistent across both body segments. The data suggests that the range of the average deviation values for the head and trunk were comparable within their respective ranges of variability. Using a similar methodology, additional studies could examine the measurement deviations in head-trunk coordination measures, such as the average orientation offset of the head from the torso.

The present analysis evaluated Theia3D and the inertial sensors in a global reference frame, therefore transformations into the anatomical reference frame would provide a more accurate interpterion of a person’s true head or torso orientation with respect to a neutral posture. Expressing the data in the anatomical reference frame could also enable normalizing the RMSD results using the anatomical functional range of motion of each body segment. The range of motion for the cervical spine is approximately up to 90° of flexion, 70° of extension, 45° of lateral flexion on either side, and up to 90° of rotation to both sides [23]. Torso range of motion is approximately 45° of flexion, 30° of extension, 40° of lateral flexion on either side, and up to 50° of transverse rotation [24]. This approach would express the error as a proportion of the total available motion, enabling easier interpretation with respect to the overall movement capacity.

Comparing the present results to existing literature is challenging due to differences in the functional tasks performed and the dependent measures evaluated; however, limited relevant results can be considered. Steffensen et al. [25] compared Theia3D to a marker-based system, using ten cameras for each, and reported trunk deviations of 2-4° across all planes during walking trials with adults who had chronic stroke and children with cerebral palsy. Among the functional tasks assessed in the present study, the CT task involved the most walking, and demonstrated reasonable agreement with an average torso deviation ranging from 1.15° to 3.60°. These findings suggest that, despite methodological differences and the diverse populations evaluated, there may be a general consistency in torso deviations during walking tasks. Future research may benefit from a concurrent analysis of Theia3D alongside inertial sensors and a marker-based motion capture system to determine variability across all three motion tracking systems.

The limited evaluation of clothing suggests a minimal influence of the flight suit on the estimation of the head and torso pose during the three tasks evaluated. The RMSD of the head estimation exhibited a 33% increase (i.e., 0.75 degrees) from unsuited to suited condition while the torso estimation resulted in a 37% increase (i.e., 1.03 degrees). As expected, the full flight suit, when worn as intended, exhibited greater deviations in the head and torso compared to the partially suited condition, where the sleeves were tied around the waist. The results suggest a potentially negligible impact of the suit on the head and trunk pose estimation similar to previous research identifying negligible impacts to gait parameters on the clinical interpretation for movement-related pathologies [12, 13]. Additional investigations are warranted with an increased sample size evaluating additional functional tasks. Understanding the potential impacts on data interpretation between postflight and preflight measures in both suited and unsuited clothing conditions is essential before incorporating the technology into operational use.

General Recommendations for Optimal Tracking—The following section provides recommendations for future system integration into spaceflight vehicles, habitats, or ground applications. An array of multiple cameras (e.g., six to eight) are recommended to surround the area of interest, enabling frontal, sagittal, and oblique views of the subject. While symmetrical camera arrays are ideal for improved accuracy, various configurations can support human tracking. In addition to physical positioning of the hardware, timecode-synchronization of the cameras is required to ensure the acquisitions take place concurrently for each camera angle. Wire-based synchronization, transferring timecodes from a master device to the remaining devices, provides the highest precision for synchronization. Alternative wireless synchronization methods may include transmitters and receivers for timecode signals, audio syncing [26], LED-based syncing with flashes of light at a consistent interval [27], and software-based syncing. Additional research will be required to develop calibration methods for in-flight data capture. Object calibrations can be performed using an object with known dimensions as an alternative to the traditional calibration board method. An adequate frame rate, proportional to the movement of interest, is also recommended. For faster movements, higher frame rates produce more accurate human pose estimations. The camera exposure should be selected based on the frame rate, following a guideline of the inverse of two-times the frame rate or higher in seconds. Regarding resolution, the subject in the capture volume should be visible and fill at least half of the camera's field of view. To properly track a body segment such as the feet, the lower limbs should be visible in three or more cameras. While skin-tight clothing is not necessary, subjects should wear clothing that is fitted to the body and colors that support visibility considering ambient light conditions. Finally, the reduction of occlusions wherever possible [28], such as eliminating undesired items in front of cameras and occlusions of multiple individuals can support superior tracking accuracy.

Limitations and Future Work—The findings from the present research should be interpreted with consideration of the following limitations. The study comprised a small sample of individuals who performed a subset of functional tasks in various environments, camera configurations, and clothing conditions. While varying anthropometry was introduced in the limited sample of subjects tested, the addition of more subjects of diverse heights, weights, and clothing conditions are warranted. The evaluation of additional functional tasks may also provide further insight into the influence of task characteristics on the accuracy of the MMC estimations. It is important to note that although inertial sensors were primarily used as the standard for accurate estimation in this comparative evaluation, IMU devices also introduce their own sources of error, such as gimbal lock where two axes align and cause a loss of one degree of freedom. In addition, the analysis focused mainly on head and trunk coordination, which is unique to the current literature. Future work could encompass comparisons to a marker-based systems during sensorimotor tasks to replicate and extend previous analysis from the current body of literature. Additionally, there is a need for future investigations of inflight evaluations or parabolic flights to determine the accuracy of MMC in weightless or partial gravity environments. Conducting investigations during spaceflight or analog settings could help pinpoint potential limitations and refine the training data used in the tracking algorithms, ultimately improving human pose estimation in these specific environments.

5. CONCLUSION

The study evaluated the performance of Theia3D, a makerless motion capture software, to inertial sensors for head and trunk pose estimations during various functional tasks and environmental conditions. The average RMSD of Theia3D compared to the inertial sensors was less than five degrees for both testing protocols, irrespective of task type and plane of motion. The research demonstrated that reducing the number of cameras from eight to six, combined with a non-symmetrical capture volume and the presence of more individuals and occlusions, led to slightly greater average deviations of head and trunk angles from the estimations provided by the inertial sensors. In general, functional tasks that required more dynamic motion and ambulation resulted in higher deviations than more stationary tasks such as postural balance. The findings suggest possible variations in tracking accuracy across different planes of motion when using fewer cameras, emphasizing the critical role of camera placement. The limited assessment of clothing indicates that the flight suit has minimal impact on the estimation accuracy of the head and torso. While the present work provides a foundation for the level of data accuracy that can be expected in suboptimal testing conditions, such as during postflight sensorimotor assessments, additional research is needed to establish the acceptable level of measurement variation.

APPENDICES

A. TABLES

Table 1. Magnitude-Squared Coherence: Theia3D vs. Inertial Sensor Head Estimations (Protocol 1)

Protocol 1 (n= 3): Magnitude Squared Coherence (Head)					
Task	Pitch	Roll	Yaw	Mean	SD
Cone Turn	0.83	0.44	0.99	0.75	0.28
Cone Turn (Fixed)	0.45	0.52	0.99	0.65	0.29
Sit to Stand	0.71	0.32	0.49	0.51	0.19
Sit to Stand (Fixed)	0.69	0.29	0.44	0.47	0.20
Tandem Eyes Closed	0.34	0.37	0.41	0.37	0.04
Mean	0.60	0.39	0.66		
SD	0.20	0.09	0.30		

Table 2. Magnitude-Squared Coherence: Theia3D vs. Inertial Sensor Torso Estimations (Protocol 1)

Protocol 1 (n= 3): Magnitude Squared Coherence (Torso)					
Task	Pitch	Roll	Yaw	Mean	SD
Cone Turn	0.42	0.62	0.94	0.66	0.26
Cone Turn (Fixed)	0.39	0.39	0.95	0.58	0.33
Sit to Stand	0.91	0.36	0.18	0.48	0.38
Sit to Stand (Fixed)	0.92	0.32	0.32	0.52	0.35
Tandem Eyes Closed	0.36	0.46	0.37	0.40	0.06
Mean	0.60	0.43	0.55		
SD	0.29	0.12	0.37		

Table 3. Magnitude-Squared Coherence: Theia3D vs. Inertial Sensor Head Estimations (Protocol 2)

Protocol 2 (n= 6): Magnitude Squared Coherence (Head)					
Task	Pitch	Roll	Yaw	Mean	SD
Feet Adj. Head Rolling	0.56	0.46	0.26	0.42	0.15
Tandem Head Rolling	0.48	0.30	0.29	0.36	0.11
Single Leg EC	0.25	0.25	0.20	0.23	0.03
Susceptibility Task	0.34	0.23	0.16	0.24	0.09
FSST	0.42	0.32	0.42	0.38	0.06
Step Test	0.34	0.31	0.29	0.31	0.02
Obstacle Turn Task	0.43	0.51	0.75	0.56	0.17
Kneel & Turn	0.46	0.29	0.57	0.44	0.14
Mean	0.41	0.33	0.37		
SD	0.10	0.10	0.20		

Table 4. Magnitude-Squared Coherence: Theia3D vs. Inertial Sensor Torso Estimations (Protocol 2)

Protocol 2 (n= 6): Magnitude Squared Coherence (Torso)					
Task	Pitch	Roll	Yaw	Mean	SD
Feet Adj. Head Rolling	0.41	0.22	0.32	0.31	0.10
Tandem Head Rolling	0.18	0.14	0.29	0.20	0.08
Single Leg EC	0.71	0.18	0.61	0.50	0.28
Susceptibility Task	0.30	0.27	0.36	0.31	0.04
Four Square Step Test	0.41	0.32	0.35	0.36	0.04
Step Test	0.20	0.43	0.29	0.31	0.11
Obstacle Turn Task	0.42	0.55	0.78	0.59	0.18
Kneel & Turn	0.69	0.53	0.36	0.52	0.17
Mean	0.42	0.33	0.42		
SD	0.20	0.16	0.18		

B. FIGURES

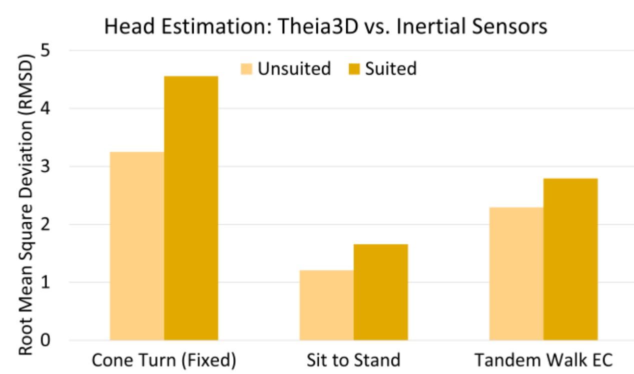

Figure 11. Suited and unsuited comparisons of RMSD results of the head averaged across all three planes of motion (n=2).

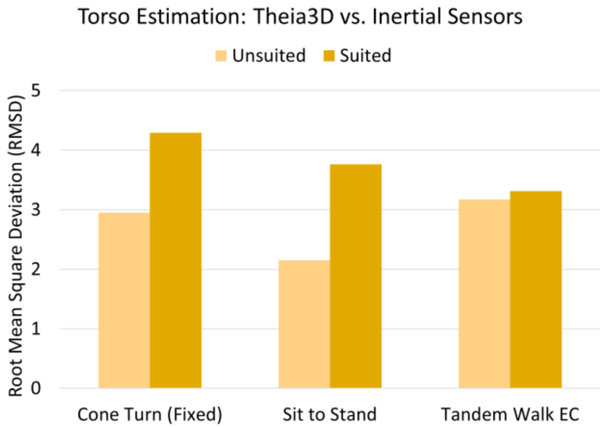

Figure 12. Suited and unsuited comparisons of RMSD results of the torso averaged across all three planes of motion (n=2).

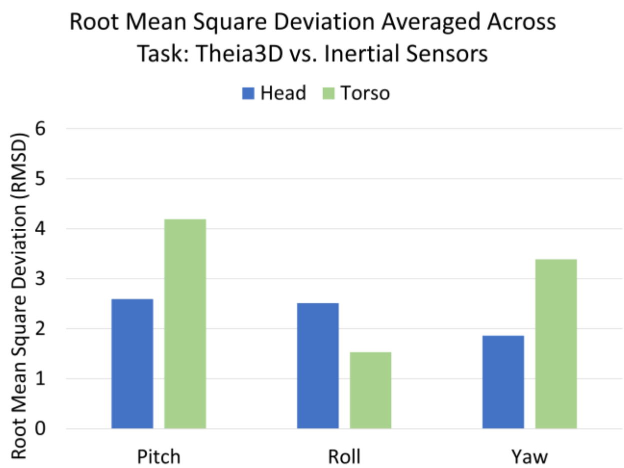

Figure 13. Protocol 1 (n=3): Root mean square deviation of Theia3D compared to inertial sensors averaged across all tasks performed.

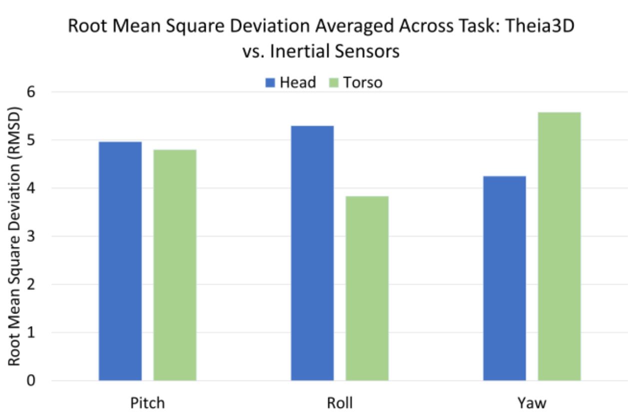

Figure 14. Protocol 2 (n=6): Root mean square deviation of Theia3D compared to inertial sensors averaged across all tasks performed.

ACKNOWLEDGEMENTS

The work was supported by the National Aeronautics and Space Administration (NASA) Exploration Systems Development Mission Directorate within the Mars Campaign Office Crew Health Countermeasures. The authors express their gratitude to the Aerospace Environment Protections Laboratory for their support in integrating the markerless motion capture system into a field-testing environment.

REFERENCES

[1] S. L. Colyer, M. Evans, D. P. Cosker, and A. I. T. Salo, "A Review of the Evolution of Vision-Based Motion Analysis and the Integration of Advanced Computer Vision Methods Towards Developing a Markerless System," *Sports Medicine - Open*, vol. 4, no. 1, p. 24, 2018/06/05 2018, doi: 10.1186/s40798-018-0139-y.

[2] R. M. Kanko, E. Laende, W. S. Selbie, and K. J. Deluzio, "Inter-session repeatability of markerless motion capture gait kinematics," *Journal of Biomechanics*, vol. 121, p. 110422, 2021/05/24/ 2021, doi: https://doi.org/10.1016/j.jbiomech.2021.110422.

[3] G. Clement, S. C. Moudy, T. R. Macaulay, M. O. Bishop, and S. J. Wood, "Mission-critical tasks for assessing risks from vestibular and sensorimotor adaptation during space exploration," *Front Physiol*, vol. 13, p. 1029161, 2022, doi: 10.3389/fphys.2022.1029161.

[4] L. Vu *et al.*, "Development of a Depth Camera-Based Instructional Tool for Resistive Exercise During Spaceflight," in *Advances in Human Factors in Sports, Injury Prevention and Outdoor Recreation*, Cham, T. Ahram, Ed., 2018// 2018: Springer International Publishing, pp. 91-99.

[5] Y. Hernandez, K. Han Kim, E. Benson, S. Jarvis, and S. Rajulu, "Video-Based Ergonomic Assessment for Spacesuit Training in a Microgravity Analog," *Proceedings of the Human Factors and Ergonomics Society Annual Meeting*, vol. 63, no. 1, pp. 987-991, 2019/11/01 2019, doi: 10.1177/1071181319631149.

[6] Y. Hernandez, K. H. Kim, E. Benson, S. Jarvis, I. Meginnis, and S. Rajulu, "Underwater space suit performance assessments part 1: Motion capture system development and validation," *International Journal of Industrial Ergonomics*, vol. 72, pp. 119-127, 2019/07/01/ 2019, doi: https://doi.org/10.1016/j.ergon.2019.04.008.

[7] K. H. Kim, Y. Hernandez, E. Benson, S. Jarvis, I. Meginnis, and S. Rajulu, "Underwater space suit performance assessments part 2: Reach envelopes as a comparative performance metric," *International Journal of Industrial Ergonomics*, vol. 73, p. 102832, 2019/09/01/ 2019, doi: https://doi.org/10.1016/j.ergon.2019.102832.

[8] L. Vu, K. Han Kim, A. Gordon, and S. Rajulu,

"Machine-learning Solution for Automatic Spacesuit Motion Recognition and Measurement from Conventional Video," presented at the 51st International Conference on Environmental Systems, St. Paul, Minnesota, 10-14 July 2022, 2022.

[9] T. Xu, "Single-view and Multi-view Methods in Marker-less 3D Human Motion Capture," *Journal of Physics: Conference Series,* vol. 1335, no. 1, p. 012022, 2019/10/01 2019, doi: 10.1088/1742-6596/1335/1/012022.

[10] K. Song, T. J. Hullfish, R. S. Silva, K. G. Silbernagel, and J. R. Baxter, "Markerless motion capture estimates of lower extremity kinematics and kinetics are comparable to marker-based across 8 movements," *bioRxiv,* p. 2023.02.21.526496, 2023, doi: 10.1101/2023.02.21.526496.

[11] B. K. Lahkar, A. Muller, R. Dumas, L. Reveret, and T. Robert, "Accuracy of a markerless motion capture system in estimating upper extremity kinematics during boxing," (in English), *Frontiers in Sports and Active Living,* Original Research vol. 4, 2022-July-25 2022, doi: 10.3389/fspor.2022.939980.

[12] M. Flood, P. Gette, J. Cabri, and B. Grimm, "MARKERLESS MOTION CAPTURE FOR CLINICAL MOVEMENT ANALYSIS AND THE INFLUENCE OF CLOTHING ON GAIT METRICS," *Orthopaedic Proceedings,* vol. 105-B, no. SUPP_9, pp. 70-70, 2023, doi: 10.1302/1358-992x.2023.9.070.

[13] V. T. Keller, J. B. Outerleys, R. M. Kanko, E. K. Laende, and K. J. Deluzio, "Clothing condition does not affect meaningful clinical interpretation in markerless motion capture," *Journal of Biomechanics,* vol. 141, p. 111182, 2022/08/01/ 2022, doi: https://doi.org/10.1016/j.jbiomech.2022.111182.

[14] S. Madansingh and J. J. Bloomberg, "Understanding the effects of spaceflight on head–trunk coordination during walking and obstacle avoidance," *Acta Astronautica,* vol. 115, pp. 165-172, 2015/10/01/ 2015, doi: https://doi.org/10.1016/j.actaastro.2015.05.022.

[15] S. A. E. Nooij, J. E. Bos, E. L. Groen, W. Bles, and W. J. Ockels, "Space sickness on earth," *Microgravity Science and Technology,* vol. 19, no. 5, pp. 113-117, 2007/09/01 2007, doi: 10.1007/BF02919464.

[16] W. Dite and V. A. Temple, "A clinical test of stepping and change of direction to identify multiple falling older adults," *Arch Phys Med Rehabil,* vol. 83, no. 11, pp. 1566-71, Nov 2002, doi: 10.1053/apmr.2002.35469.

[17] K. D. Hill, "A new test of dynamic standing balance for stroke patients: Reliability, validity and comparison with healthy elderly," *Physiother. Can.,* vol. 48, no. 4, pp. 257-262, 1996/10 1996, doi: 10.3138/ptc.48.4.257.

[18] H. Weiss, Y. Hernandez, K. H. Kim, and S. L. Rajulu, "3D virtual fit assessment and modeling: liquid cooling and ventilation garment," *International Journal of Clothing Science and Technology,* vol. 34, no. 3, pp. 301-314, 2022, doi: 10.1108/IJCST-09-2020-0143.

[19] K. Wishaupt, W. Schallig, M. H. van Dorst, A. I. Buizer, and M. M. van der Krogt, "The applicability of markerless motion capture for clinical gait analysis in children with cerebral palsy," *Scientific Reports,* vol. 14, no. 1, p. 11910, 2024/05/24 2024, doi: 10.1038/s41598-024-62119-7.

[20] J. L. McGinley, R. Baker, R. Wolfe, and M. E. Morris, "The reliability of three-dimensional kinematic gait measurements: A systematic review," *Gait & Posture,* vol. 29, no. 3, pp. 360-369, 2009/04/01/ 2009, doi: https://doi.org/10.1016/j.gaitpost.2008.09.003.

[21] J. J. Bloomberg, B. T. Peters, S. L. Smith, W. P. Huebner, and M. F. Reschke, "Locomotor head-trunk coordination strategies following space flight," *J Vestib Res,* vol. 7, no. 2-3, pp. 161-77, Mar-Jun 1997. [Online]. Available: https://www.ncbi.nlm.nih.gov/pubmed/9178222.

[22] A. P. Mulavara *et al.,* "Vestibular-somatosensory convergence in head movement control during locomotion after long-duration space flight," *Journal of Vestibular Research,* vol. 22, pp. 153-166, 2012, doi: 10.3233/VES-2011-0435.

[23] E. E. Swartz, R. T. Floyd, and M. Cendoma, "Cervical spine functional anatomy and the biomechanics of injury due to compressive loading," *J Athl Train,* vol. 40, no. 3, pp. 155-61, Jul-Sep 2005. [Online]. Available: https://www.ncbi.nlm.nih.gov/pubmed/16284634.

[24] W. Gao and M. Ceccarelli, "Design and Performance Analysis of LARMbot Torso V1," *Micromachines,* vol. 13, p. 1548, 09/18 2022, doi: 10.3390/mi13091548.

[25] E. A. Steffensen, F. Magalhães, B. A. Knarr, and D. C. Kingston, "Comparison of markerless and marker-based motion capture of gait kinematics in individuals with cerebral palsy and chronic stroke: A case study series," *Res. Sq.,* 2023/2/8 2023, doi: 10.21203/rs.3.rs-2557403/v1.

[26] P. Shrstha, M. Barbieri, and H. Weda, "Synchronization of multi-camera video recordings based on audio," presented at the Proceedings of the 15th ACM international conference on Multimedia, Augsburg, Germany, 2007. [Online]. Available: https://doi-org.proxy.lib.umich.edu/10.1145/1291233.1291367.

[27] X. Ding and P. Tao, "Synchronization Detection of

Multicamera System Based on LED Matrix," in *2016 13th International Conference on Embedded Software and Systems (ICESS)*, 13-14 Aug. 2016 2016, pp. 18-23, doi: 10.1109/ICESS.2016.13.

[28] L. Wade, L. Needham, P. McGuigan, and J. Bilzon, "Applications and limitations of current markerless motion capture methods for clinical gait biomechanics," *PeerJ*, vol. 10, no. e12995, p. e12995, 2022/2/25 2022, doi: 10.7717/peerj.12995.

BIOGRAPHY

Hannah Weiss *is senior human factors engineer and scientist within the Neuroscience Laboratory at the NASA Johnson Space Center. She earned her Ph.D. from the University of Michigan in Industrial and Operations Engineering in 2024.*

Sarah Moudy *is a senior scientist within the Neuroscience Laboratory at the NASA Johnson Space Center. She earned her Ph.D. in Sport Science: Biomechanics and Neuromuscular Physiology from the University of Roehampton in 2019.*

Scott Wood *is the Neuroscience Laboratory Director at the NASA Johnson Space Center. He earned his Ph.D. in 2000 from Baylor College of Medicine in Audiology & Bioacoustics*